International Journal of Psychosocial Rehabilitation, Vol. 24, Issue 05, 2020
ISSN: 1475-7192

Lossless Medical Image Compression by Multi Oriented Prediction Technique

P. Renukadevi and Dr.M. Syed Mohomed

Abstract--- *Image compression plays a vital role in medical field in which the medical images can be transmitted from one place to another, needs less space to store the data. Radiologist scans the patient's interior part of the body by using some technology and instruments. Medical images are in the form of X-ray, CT, MRI, PET etc. In hospitals and health centers large amounts of medical image data are produced during the diagnosis of the patient. The proposed algorithms are tested over 325 cases of 3D medical images. The experimental results reveals that proposed image compression then encryption system provides high compression ratio, better bits per pixel, mean square error, less encryption and decryption time with better encryption quality and good system performance as compared to existing approaches. The PSNR value for 3D medical image is 56.4754 and the CT image PSNR value is 55.3924.*

Keywords--- *Multi Oriented Prediction Technique, Lossless Medical Image Compression.*

I. LITERATURE SURVEY

The field of image compression has increased because of expanding the requirements for transmission of image in computer, mobile environments and the field of image compression is significantly increased. The presentation of existing strategies or literature survey in this research work is to examine the digital image processing based on compression and prediction particularly in near lossless image compression and near lossless image prediction. Image compression is the key component in signal processing and communication systems. Reduction of storage space, transmission bandwidth and cost are possible in image compression. These compression and prediction of images are retrieval and analyses the image processing parameters based on the various algorithms.

DT-CWT and SPIHT based new image compression algorithm. SPIHT algorithm based on the relationship between the initial threshold and the target bitrate is used to reduce required memory space and the computation time. Computational efficiency properties and good directional selectivity makes DT-CWT good candidate for image compression but the compression ratio is low [1].

Vector Quantization (VQ) and Discrete Cosine Transform (DCT) based lossy image compression method. It also presented new lossy image compression method that combines DCT and wavelet transform for obtaining better visual quality of images and higher compression ratio but the processing speed is low [2].

Wavelet transform based image compression technique that removes blocking artifacts which are present in DCT. Also he had compared the different wavelet families like Daubechies, Biorthogonal, Haar, Symlets, Coiflets, and Reverse Biorthogonal for various images but the redundancy was high [3].

P. Renukadevi, Research Scholar, Manonmaniam Sundaranar University, Tirunelveli, Tamil Nadu.
Dr.M. Syed Mohomed, Assistant Professor, Department of Computer Science, Sri Ram Nallamani Yadava College of Arts and Science, Tenkasi, Tamil Nadu.

DOI: 10.37200/IJPR/V24I5/PR201800
Received: 13 Feb 2020 | Revised: 07 Mar 2020 | Accepted: 23 Mar 2020

A lossless image compression algorithm use run length encoding method for compression. This compression technique proves to be highly effective for images with large similar locality of pixel lay out. This technique has some complexity in execution [4].

Novel technique for the lossy, which is combination of vector quantization and Discrete Wavelet Transform, to achieve higher quality of reconstruction image at low bitrates and fast decoding, but higher time complexity for encoding. The performance of this technique enhanced when it is used with the linear vector quantization but the efficiency is low [5].

The image compression technique by utilizing Discrete Cosine Transform. It is a JPEG compression algorithm which is utilized for full-color still image applications and describes all the component present in the image compression is used for managing images in digital format with higher loss in pixels [6].

A solar power prediction model with the help of various satellite images and a support vector machine (SVM) learning scheme.. An AMV extraction method is used to gather the information of wind direction and speed. An extraction method of cloud factors from the satellite images to specify a target area and a search area. Finally, a training method is used with SVM regression. The advantage of this is, it shows the highest prediction accuracy and simultaneously predict the future amount of clouds and solar irradiance [7].

An algorithm for sonar image prediction based underwater hovering. The FLS model is introduced and the sonar image coordinates are defined using the parameters like minimal range, maximal range and field-of-view. The next step followed is the sonar-image prediction method. The advantage is that it reduces the position error of the surge and sway directions when underwater objects are investigated to maintain the position of AUV [8].

Region based prediction for image compression for cloud storage. Inter-image correlations are exploited using semi-local approach. The reference image is first segmented into multiple planar regions. The references are organized in a pseudo sequence to differentially encode the input image using classical video coding tools the encoding bits are must be rearranged for accurate result [9].

Using Chaos Masking (CMS) technique the encryption was performed. This method improves the security because the key space is large but possibility of mismatched pixel is obtained during processing [11].

II. PROPOSED ARCHITECTURE

Figure 1 is the block diagram of the proposed architecture. In the first step image is acquired from the instrument by the physician. The CT, MRI, PET scan image are taken in data base. Before compressing the image, the medical image is preprocessed to remove the noise. In this proposed architecture Recursive Least Square Mean filter is used to remove the noise of the image. In the second step Multi-directional Gradient Oriented Prediction (MGOP) technology is used. It splits the medical image into high resolution image and low resolution image and easily predicts the nearest pixel of the image. This improves the prediction efficiency since the prediction is applied to different orientations. These predictors are optimized to predict sharp horizontal edge, sharp vertical edge, horizontal edge, weak horizontal edge, vertical edge and weak vertical edges.

DOI: 10.37200/IJPR/V24I5/PR201800
Received: 13 Feb 2020 | Revised: 07 Mar 2020 | Accepted: 23 Mar 2020

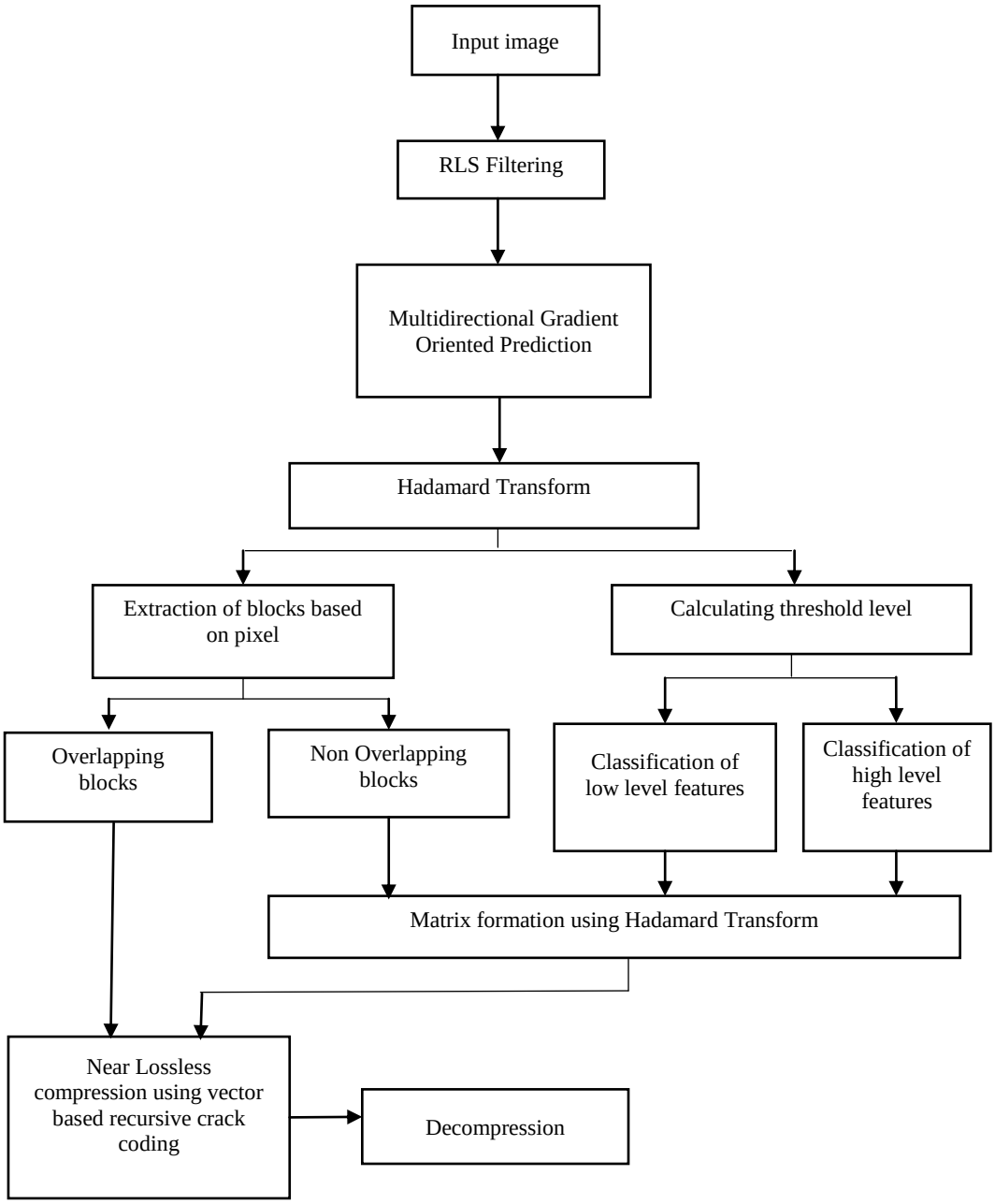

Figure 1: Block Diagram of Proposed Architecture

In the third step, Hadamard Transform is used to perform the compression of the image. Hadamard Transform converts the matrix form of the image and extracts the blocks based upon the pixel and then calculates the threshold value of the image. This transform is used to find the overlapping blocks and non-overlapping blocks of the matrix form of the image and also calculate low feature and high feature of the image. Overlapping block directly enters into compression and the other is used to form matrix formation.

DOI: 10.37200/IJPR/V24I5/PR201800
Received: 13 Feb 2020 | Revised: 07 Mar 2020 | Accepted: 23 Mar 2020

In the fourth step, Near-lossless compression takes place by vector based recursive crack algorithm. This provides faster compression than the previous technique. Decompression takes place by doing the steps reversely. Decompressed medical image is used for investigating and diagnosing by doctor or radiologist.

2.1 Image Acquisition

Medical images are pictures of distributions of physical attributes captured by an *image acquisition* system. Most of today's *images* are digital. They may be post-processed for analysis by a computer-assisted method. Medical image may be CT, MRI, PET, X-ray, ECG, EEC etc.

2.2 Pre-processing

During scanning process, the machine causes some noise or the patient movement or from the vibration of machine or camera setting or environmental noise or some other noise affects the medical image. To remove the unwanted disturbance of the image, first the input image is pre-processed with the help of denoising the image. Filtering techniques are performed to remove the noise of the image. Here, Recursive Least square mean adaptive filter is accepted to de-noise the image. Denoising is a vital role in image compression.

2.2.1 Recursive Least Square Mean Adaptive Filter

De-noise is an important concept in compression technique because noise occurs during the scan of the patient's inner body, movement of the patient, vibration of the scanning instrument, camera setting and environmental disturbance; all these disturbances affect the medical input image like CT/MRI. Recursive Least Squares Adaptive Filter for the removal of noise.

The initial condition is enumerated from the previously done data and the old data estimate updates by new information data. Based upon the data variable the length of the data also varies. The main aim of this filter is to reduce the mean square error.

Adaptive filter, the advantage of this filter is to provide good computational speed, system performance and the cost function is minimized. RLS helps to solve complex problem by adaptive filter. It is defined as,

$$x(k) = \sum_{n=0}^{q} b_k(n) d(k-n) + v(k) \quad (1)$$

Where, *v(k)* be additive noise. $b_k(n)$ is the binary representation.

The desired signal d(k) is given as,

$$d(k) \approx \sum_{k=0}^{p} w(n) x(k-n) = W^T X_k \quad (2)$$

Where, X_k be the column vector

$$\hat{d}(k) = \sum_{n=0}^{p} W_k(n) x(k-n) = W_k^T X_k \quad (3)$$

where w be the filter parameter, W_k be the current estimate, W_k^T be the row vector .

DOI: 10.37200/IJPR/V24I5/PR201800
Received: 13 Feb 2020 | Revised: 07 Mar 2020 | Accepted: 23 Mar 2020

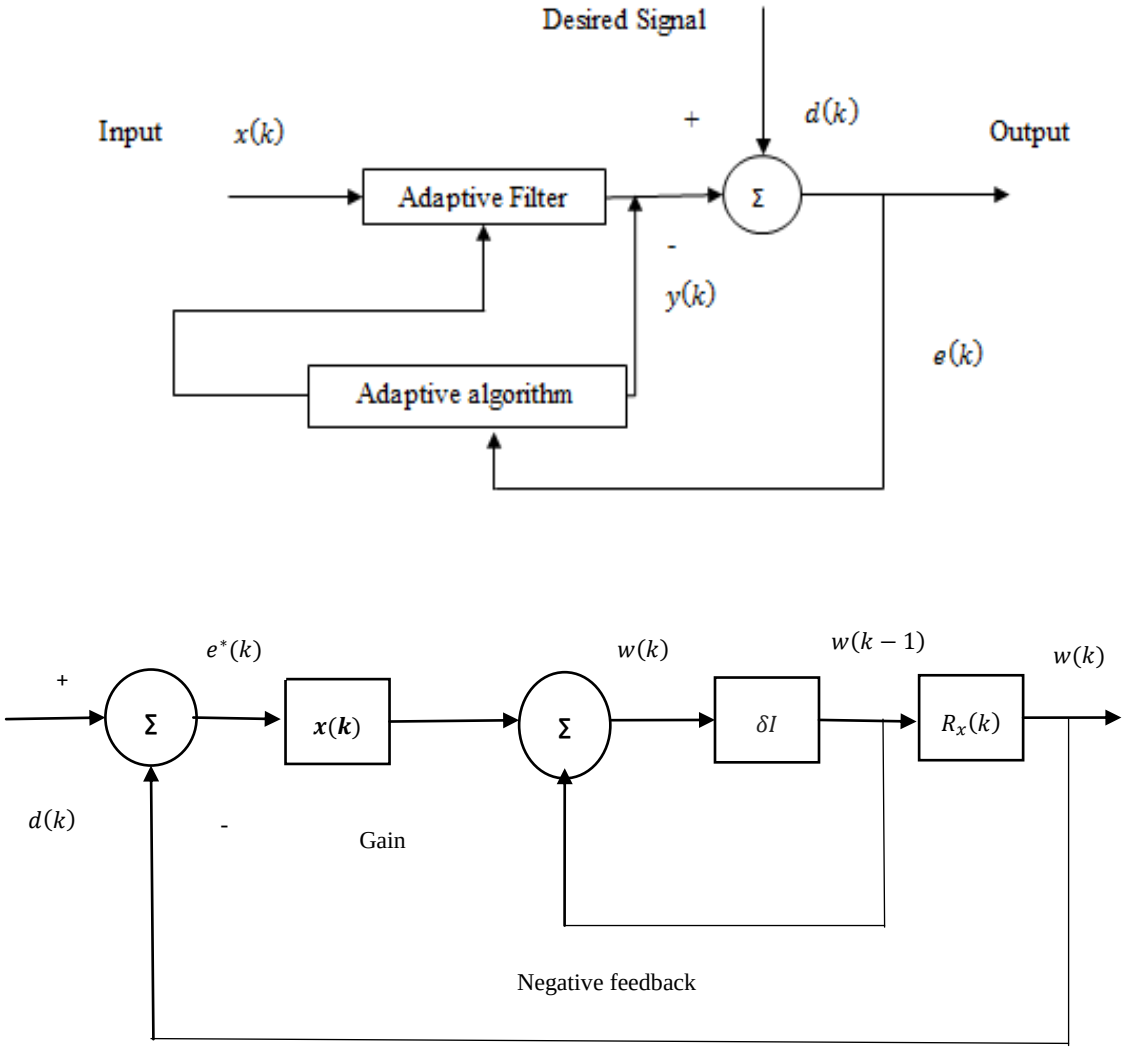

Figure 2: Signal Flow Graph of RLS Adaptive Filter

For good estimate $\hat{d}(k) - d(k)$ are small in magnitude and least square sense. It also reduces the cost function C by fixing the W_k coefficient of filter. The error signal $e(k)$and $d(k)$ are estimated in negative feedback. Figure 2 is the signal flow graph of recursive least mean square adaptive filter.

The error signal $e(k)$ can be expressed as,

$$e(k) = d(k) - \hat{d}(k) \tag{4}$$

The cost function of weighted least square error can be estimated as,

$$C(w_k) = \sum_{i=0}^{k} \lambda^{k-i} e^2(i) \tag{5}$$

Where for getting factor be $0<\lambda\leq 1$

The cost function is decreased by applying the derivative of n entries and the coefficient vector w_k and the result of settling time is zero.

DOI: 10.37200/IJPR/V24I5/PR201800
Received: 13 Feb 2020 | Revised: 07 Mar 2020 | Accepted: 23 Mar 2020

$$\frac{\partial C(W_k)}{\partial w_k(n)} = \sum_{i=0}^{k} 2\,\lambda^{k-i} e(i)\,\frac{\partial e(i)}{\partial w_k(n)} = -\sum_{i=0}^{k} 2\lambda^{k-i} e(i)x(i-n) = 0 \quad (6)$$

Where *n=0,1,…,p*

Apply *e(k)* error signal to Equation (4)

$$\sum_{i=0}^{k} \lambda^{k-i}\left[d(i) - \sum_{l=0}^{p} w_n(l)x(i-l)\right]x(i-n) = 0 \quad (7)$$

Where, *n=0,1…,p*

After rearranging the equation is,

$$\sum_{l=0}^{p} w_k(l)\left[\sum_{i=0}^{k} \lambda^{k-i}\, x(i-l)x(i-n)\right] = \sum_{i=0}^{k} \lambda^{k-i} d(i)x(i-k) \quad (8)$$

The above equation can be rewritten as matrix form,

$$R_x(k)w_k = r_{dx}(k) \quad (9)$$

Where, $R_x(k)$ be the weighted sample covariance matrix

$r_{dx}(k)$be the cross-covariance between $d(k)$ and *x(k).*

$$w_k = R_x^{-1}(k)r_{dx}(k) \quad (10)$$

Equation (4.10) is to decrease the cost function and this is the main result.

Algorithm for Recursive Least Square Mean Adaptive Filter

The algorithm for Recursive Least square mean adaptive filter for p^{th} order is as follow,

Parameter are, *p* be the filter order

λ be the forgetting factor

∂be the initialize valueP(0)

Step 1: Initialize all the parameter

$$w(k) = 0,$$
$$x(n) = 0, where\ n = -p, \ldots\ldots, -1,$$
$$d(n) = 0, where\ n = -p, \ldots\ldots, -1$$

P(0)= $\delta I, where\ Identity\ matrix\ be\ I\ of\ rank\ p+1$

Step 2: After initialization of all parameter which is pre-defined, then the computation process takes place for *k=1,2,…..p*

$$x(n) = \begin{bmatrix} x(k) \\ x(k-1) \\ \vdots \\ x(k-p) \end{bmatrix} \quad (11)$$

$$\propto (k) = d(k) - x^T(k)w(k-1) \quad (12)$$

$$g(k) = P(k-1)x(k)\{\lambda + x^T(k)P(k-1)x(k)\}^{-1} \quad (13)$$

$$P(k) = \lambda^{-1}P(k-1) - g(k)x^T(k)\lambda^{-1}P(k-1) \quad (14)$$

DOI: 10.37200/IJPR/V24I5/PR201800
Received: 13 Feb 2020 | Revised: 07 Mar 2020 | Accepted: 23 Mar 2020

$$w(k) = w(k-1) + \propto (k)g(k) \quad (15)$$

The main advantage of this filter is to remove the noise signal of the image, reduce the least mean square of the image and improve the computational speed and system performance.

2.3 Multidirectional Gradient Oriented Prediction (MGOP)

A Multidirectional Gradient Oriented Prediction (MGOP) Scheme based on least square estimation is used to provide better near-lossless compression improvements. In this method MOP is used along with Gradient Adjusted Prediction. Edges as well as smooth areas in the medical images are predicted using MGOP. The Figure 3 shows the contextual prediction pattern for the prediction in MGOP.

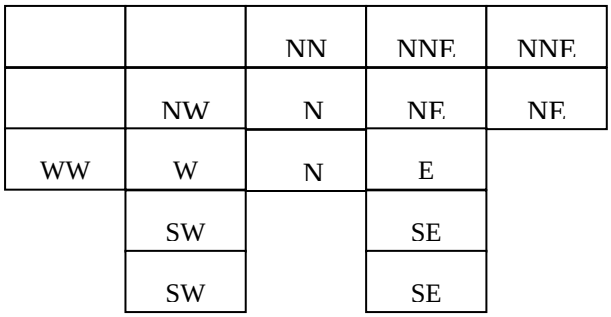

Figure 3: Contextual Prediction Pattern for the Prediction in MGOP

Algorithm for MGOP

1. Input the Original Image
2. Apply RLS filtering.
3. Apply MGOP

i) Step 1 → Residual 0

ii) Step 2 → Residual 1

4. Calculate H, V, Hybrid_HV, π /4, 3 π /4 and Hybrid _ Diagonal Predictor coefficients.
5. Calculate dh =|W-WW| +|N-NW|

dv=|W-NW| +|N-NN| +|NE-NNE|

6. Calculate best Orientation ‘f”
7. Calculate $\hat{x}$ based on f, dh and dv.

i) If f= H then $\hat{x}$= N

ii) If f=V then $\hat{x}$ = (W+S)/2

iii) If f= Hybrid_HV then $\hat{x}$ = (N+W+S)/2

iv) If f= π /4 then $\hat{x}$= (SW+NE)/2

DOI: 10.37200/IJPR/V24I5/PR201800
Received: 13 Feb 2020 | Revised: 07 Mar 2020 | Accepted: 23 Mar 2020

v) If f=3 π /4 then x̂= (NW+SE)/2

vi) If f= Hybrid-_Diagonal then

$$\hat{x} = \frac{N + W + \frac{1}{\sqrt{2}}(NW + NE + SW + SE)}{3 + \frac{4}{\sqrt{2}}}$$

vii) If(dv-dh >80) then $\hat{x}$ =W

Else (dv-dh< - 80) then $\hat{x}$=N

Else $\hat{x}$= (W+N/ 2) + (NE-NW)/4

viii) If (dv-dh >32) then x̂= (x̂+W)/2

Else If (dv-dh> 8) then $\hat{x}$= (3$\hat{x}$+W)/4

Else If (dv-dh < -32) then $\hat{x}$= ($\hat{x}$+N)/2

Else If (dv-dh < -8) then $\hat{x}$= (3$\hat{x}$+N)/4

8. Calculate Prediction Error $e_{i,j} = x_{i,j} - \bar{x}_{i,j}$

9. Apply Hadamard Transform

10. Compress the medical image using Vector Based Recursive crack coding.

"The digital implementation of a filter is lossless if the output is the result of a digital one-to-one operation on the current sample and the recovery processor is able to construct the inverse operator."

2.4 Hadamard Transform (Ht)

Hadamard Transform (HT) has low compression efficiency. It is however, speedy, since it can be computed and implemented with just additions, subtractions, and an occasional right shift. Given an N × N block of pixels Pxy (where N must be a power of 2, N=2n) its two dimensional HT and Inverse HT are defined by Equation (17) and Equation (19) respectively:

$$H(u,v) = \sum_{x=0}^{N-1}\sum_{y=0}^{N-1} pxy\ g\ (x,y,u,v) \quad (16)$$

$$= \frac{1}{N}\sum_{x=0}^{N-1}\sum_{y=0}^{N-1} pxy\ \ (-1)\sum_{i=0}^{n-1}[bi(x)pi(u) + bi(y)pi(v)] \quad (17)$$

$$Pxy = \sum_{x=0}^{N-1}\sum_{y=0}^{N-1} H\ (u,v)\ \ h\ (x,y,u\ v) \quad (18)$$

$$= \frac{1}{N}\sum_{x=0}^{N-1}\sum_{y=0}^{N-1} H(u,v)\ \ (-1)\sum_{i=0}^{n-1}[bi(x)pi(u) + bi(y)pi(v)] \quad (19)$$

$$P_0(u) = b_{n-1}(u),$$

$$P_1(u) = b_{n-1}(u) + b_{n-2}(u)$$

$$P_2(u) = b_{n-2}(u) + b_{n-3}(u)$$

$$P_{n-1}(u) = b_1(u) + b_0(u) \quad (20)$$

The quantities g(x, y, u, v) and h(x, y, u, v) are kernels of HT. These matrices are identical. They consist of +1 and -1 and they are multiplied by the factor 1/N.

DOI: 10.37200/IJPR/V24I5/PR201800
Received: 13 Feb 2020 | Revised: 07 Mar 2020 | Accepted: 23 Mar 2020

In this proposed framework, Hadamard transform is used to reduce the redundancy in compressed image as well as to remove the blocking artifacts. The Hadamard transform is a symmetric system, separable unitary transformation it has only two elements in its kernel matrix are +1 and -1. The Hadamard transform is existing for $N = 2^n$ in which n represents the integer. Jeyathilake *et al.* (2013) presented the Hadamard Transform (HT).

The kernel matrix for these two cases is given below:

$$\frac{1}{\sqrt{2}}H_2 = \frac{1}{\sqrt{2}}\begin{bmatrix}1 & 1\\ 1 & -1\end{bmatrix} \quad (21)$$

For larger N, it can be created from block matrix form is:

$$\frac{1}{\sqrt{N}}H_N = \frac{1}{\sqrt{N}}\begin{bmatrix}H_{N/2} & H_{N/2}\\ H_{N/2} & -H_{N/2}\end{bmatrix} \quad (20)$$

The matrix contains only element that are 1 for size $N = 2^n$, it makes the transform very less expensive.

If N=8, the Hadamard kernel matrix is given as:

$$H_8 = \frac{1}{2\sqrt{2}}\begin{bmatrix}1 & 1 & 1 & 1 & 1 & 1 & 1 & 1\\ 1 & -1 & 1 & -1 & 1 & -1 & 1 & -1\\ 1 & 1 & -1 & -1 & 1 & 1 & -1 & -1\\ 1 & -1 & -1 & 1 & 1 & -1 & -1 & 1\\ 1 & 1 & 1 & 1 & -1 & -1 & -1 & -1\\ 1 & -1 & 1 & -1 & -1 & 1 & -1 & 1\\ 1 & 1 & -1 & -1 & -1 & -1 & 1 & 1\\ 1 & -1 & -1 & 1 & -1 & 1 & 1 & -1\end{bmatrix}\begin{matrix}0\\7\\3\\4\\1\\6\\2\\5\end{matrix} \quad (21)$$

In the above matrix the number of sign changes shown in column to the right corresponding to row. This sign change count is representing asthe sequence of the row.

2.5 Vector based Recursive Crack Coding Image Compression

In the first phase, the codebook for given image is created

In the second phase, the codebook is given as an input with original image for compression.

The approach of vector introduced in the recursive crack coding is to make the algorithm faster than the existing algorithm for a given level of compression. The vector introduces the vector encoding where it scan all the pixels in the input image and make the codebook.

The vector quantization is the generalization of k-means in which the input image is divided into disjoint sub-images and then encoded the original image as the concatenation of the code for the sub-images or sub-vector. The distance between the sub-images of SM and the selected centroids for each corresponding sub-images of C is given the full distance. The goal of the vector quantization is to construct the distance d and two encoding functions.

Let us assume the distance d function is written as:

$$d(SM, C) = f\left(\sum_{j=1}^{J}\delta\left(SM_j, C_j\right)\right) \quad (22)$$

Where $f: R \to R, \delta: R \times R \to R$. The one partition the indices J into M disjoint subsets are$\{p_1, \dots, p_M\}$. The each subset is represented by sequence of J/M consecutive indices. The f is written as:

DOI: 10.37200/IJPR/V24I5/PR201800
Received: 13 Feb 2020 | Revised: 07 Mar 2020 | Accepted: 23 Mar 2020

$$\sum_{m=1}^{M}\sum_{j\in p_m}\delta\left(SM_j, C_j\right) = \sum_{m=1}^{M}\delta\left(SM^{(m)}, C^{(m)}\right) \quad (23)$$

In the above equation $SM^{(m)}, C^{(m)}$ represents the sub-vector or sub-image created by gathering of element SM and C at the indices$j \in p_m$, in each dimension of image is applied to the summing function of δ. This vector quantization replace $SM^{(m)}$ with one vector $v_i^{(m)}$ from a codebook set CD_m of possibilities. This is given as:

$$\sum_{m=1}^{M}\delta\left(SM^{(m)}, C^{(m)}\right) \approx \sum_{m=1}^{M}\delta\left(SM^{(m)}, v_i^{(m)}\right) \quad (24)$$

The above equation allows only storing the index of codebook vector instead of element of original vector$C^{(m)}$.

Let set of codebook is defined as $CD = \{CD_1, \ldots, CD_M\}$ in which each codebook represents the set of K vectors are $v_i^{(m)}, v_k^{(m)}$.

The encoding function is defined as:

$$E(c) = [i_1;, \ldots, ; i_M] \text{ Where } i_m = arg\min_i d\left(v_i^{(m)}, C^{(m)}\right) \quad (25)$$

$E(c)$is a vector and the centroid in the codebook m is given as $E(c)_m$ to near to $C^{(m)}$.

The fast encoding process and distance is obtained by using this codebook. The encoding space G be$R^{K\times M}$ and describe $D = g(SM)$as:

$$D_{im} = \delta\left(SM^{(m)}, v_i^{(m)}\right) \quad (26)$$

The right hand side of the equation is written as:

$$\sum_{m=1}^{M} D_{i/m}, i = E(c)_m \quad (27)$$

The distance can be reduced by the computation of distance between $SM^{(m)}$ and the codebook vector $v_i^{(m)}$ to approximate the centroid C. The distance between the $SM^{(m)}$ and K centroids in the codebook CD_M is defined by M columns of D.

The distance computation given by iteration through the columns, the distance in row $E(c)_m$ is added into running total. Finally the function f is reintroduced into:

$$\hat{d}\left(E1(SM).E(C)\right) = f\left(\sum_{m=1}^{M} D_{im,i} = E(c)_m\right) \quad (28)$$

Where E1 and E are the two encoding function.

Thus the vector quantization scans the original image based on two encoding functions such as codebook and centroid vector. Due to this, the computation cost is reduced.

This scanned image is given into recursive crack code for image compression. The below algorithm defines the vector based recursive crack code image compression.

Step 1: Read the scanned original image file

Step 2: The number of rows and columns in the given image is calculated.

Step 3: Separate the row and column pixels as $I[n, m]$

Step 4: For i=1 to n do 5 ## for loop is started (row pixel)

DOI: 10.37200/IJPR/V24I5/PR201800
Received: 13 Feb 2020 | Revised: 07 Mar 2020 | Accepted: 23 Mar 2020

Step 5: For j=1 to m do ## column pixel

Store $I[i,j]$ and its grey value g as the beginning of the contour

Mark the obtained pixel $I[i,j]$

Crack Code(I,i,j,g)

Step 6: The header information is noted and the contour code is noted in another file

Crack Code algorithm is started

Begin

$$\text{If}(I[i,j-1]\ equal\ g)\ then\ store\ 0; crack\_code(I,i,j-1,g);$$
$$\text{Else if}(I[i-1,j]\ equal\ g)\ then\ store\ 1; crack\_code(I,i-1,j,g);$$
$$\text{Else if}(I[i,+1j]\ equal\ g)\ then\ store\ 2; crack\_code(I,i,j+1,g);$$
$$\text{Else if}(I[i+1,j]\ equal\ g)\ then\ store\ 3; crack\_code(I,i+1,j,g);$$

Else return

End;

III. RESULTS AND DISCUSSIONS

This chapter discusses the analysis of encryption and compression of medical image by using MBKGD-LBG scheme. Various types of medical images are taken as the inputs and they have high resolution and size. Totally 5 3D medical images are taken for image compression purpose in cancer archive dataset. Medical image is nothing to examine the interior structure of the body. Different types of medical images can be taken from different instruments and different technologies. These images are investigated by doctors or radiologists who scan the image with the help of instruments. The input image is decomposed using Discrete Wavelet Transform. Here, 'haar' wavelet is used to perform the decomposition process. The medical images are compressed using LBG (Linde, Buzo, and Gray) method. Then, the image encryption is done by using Multi-round Binary key generation with Diffusion method (MBKGD).

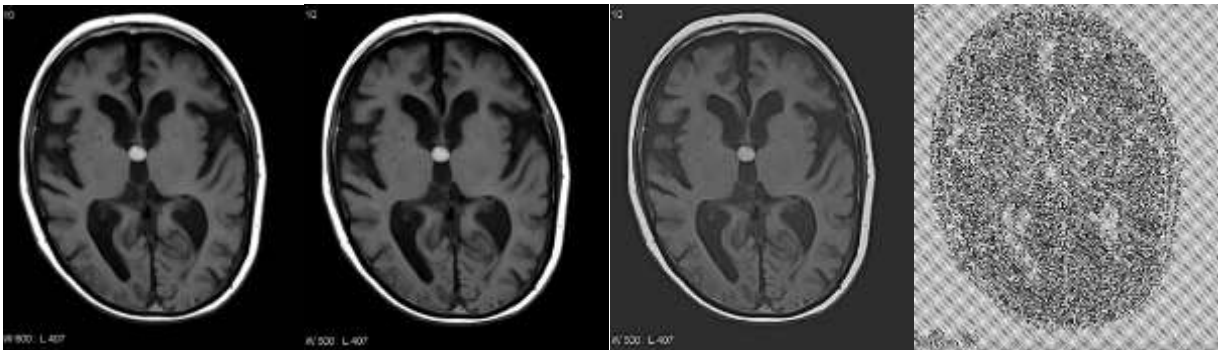

(a) (b) (c) (d)

DOI: 10.37200/IJPR/V24I5/PR201800
Received: 13 Feb 2020 | Revised: 07 Mar 2020 | Accepted: 23 Mar 2020

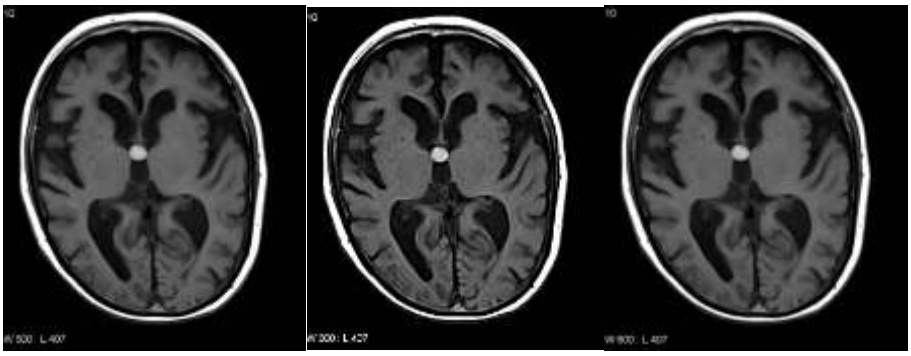

(d) (e) (f)

Figure 4: MBKGD-LBG Algorithm based Medical Brain Image Sample 1 (a) Input Image (b) Wavelet Decomposed Image (c) Compressed Image (d) Encrypted Image (e) Decrypted Image (f) Decompressed Image (g) Wavelet Reconstructed Image

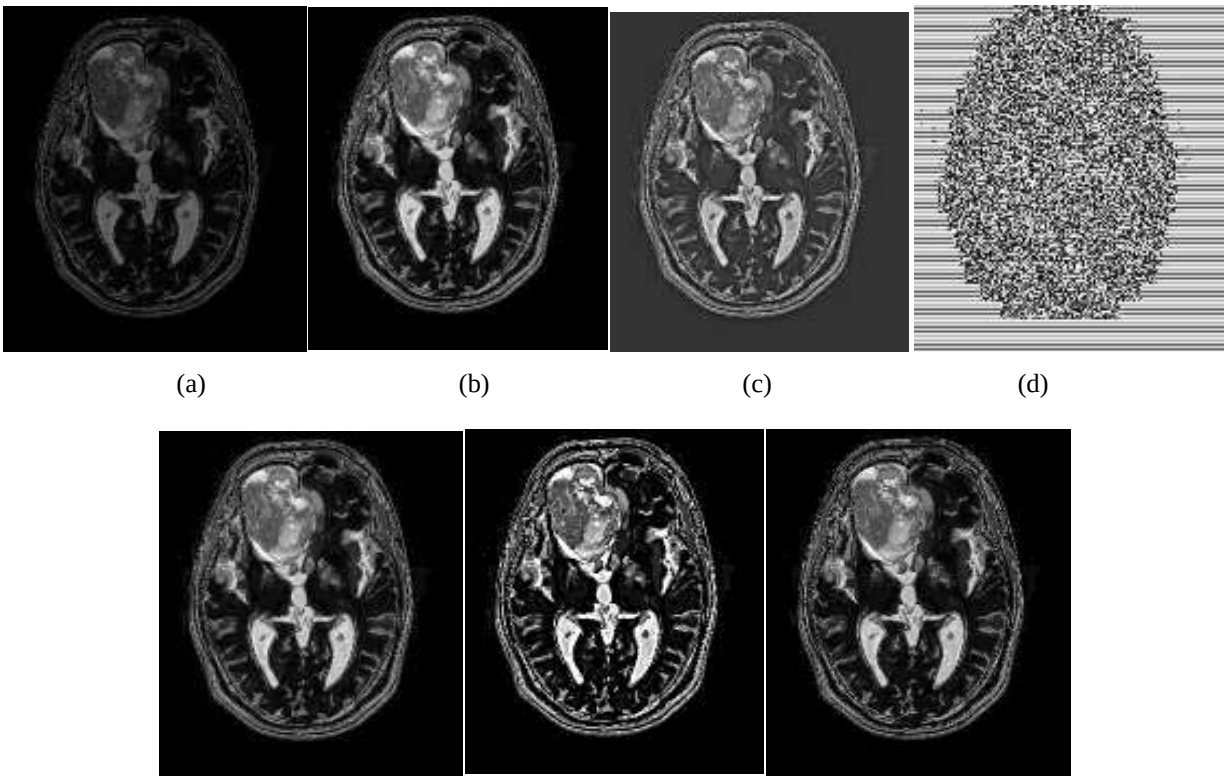

(a) (b) (c) (d)

(d) (e) (f)

Figure 5: MBKGD-LBG Algorithm based Medical Brain Image Sample 2 (a) Input Image (b) Wavelet Decomposed Image (c) Compressed Image (d) Encrypted Image (e) Decrypted Image (f) Decompressed Image (g) Wavelet Reconstructed Image

DOI: 10.37200/IJPR/V24I5/PR201800
Received: 13 Feb 2020 | Revised: 07 Mar 2020 | Accepted: 23 Mar 2020

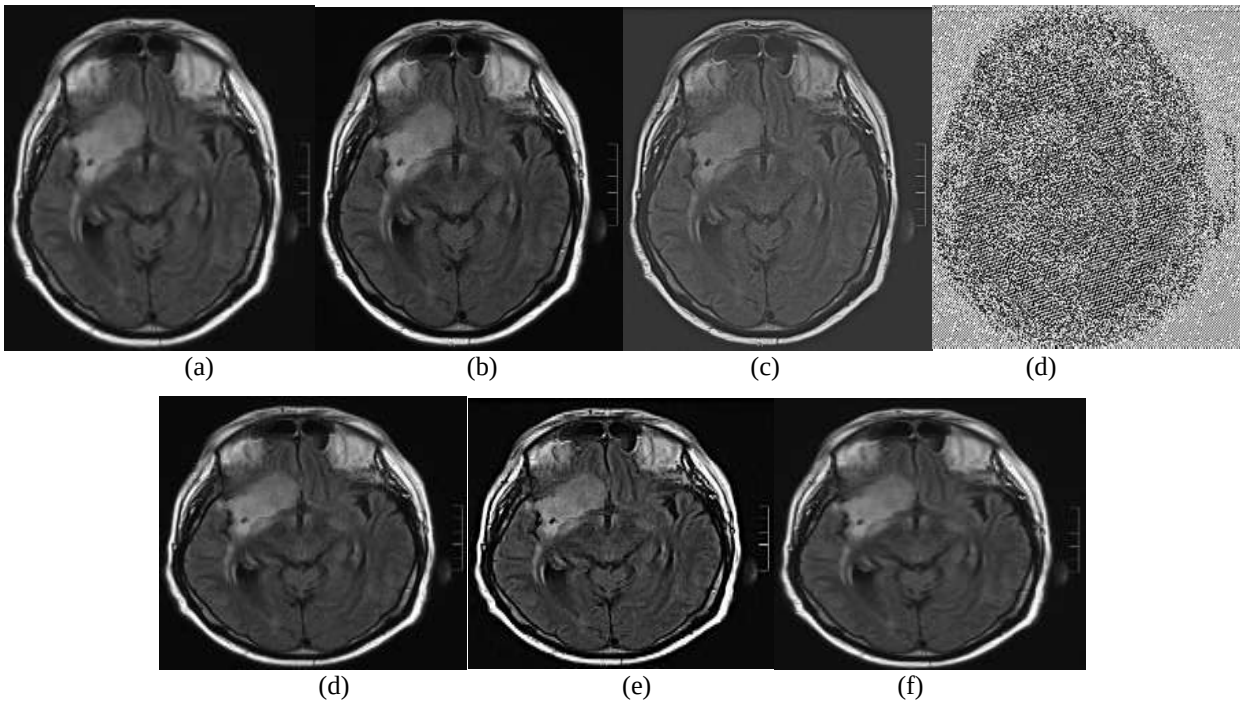

Figure 6: MBKGD-LBG Algorithm based Medical Brain Image Sample 3 (a) Input Image (b) Wavelet Decomposed Image (c) Compressed Image (d) Encrypted Image (e) Decrypted Image (f) Decompressed Image (g) Wavelet Reconstructed Image

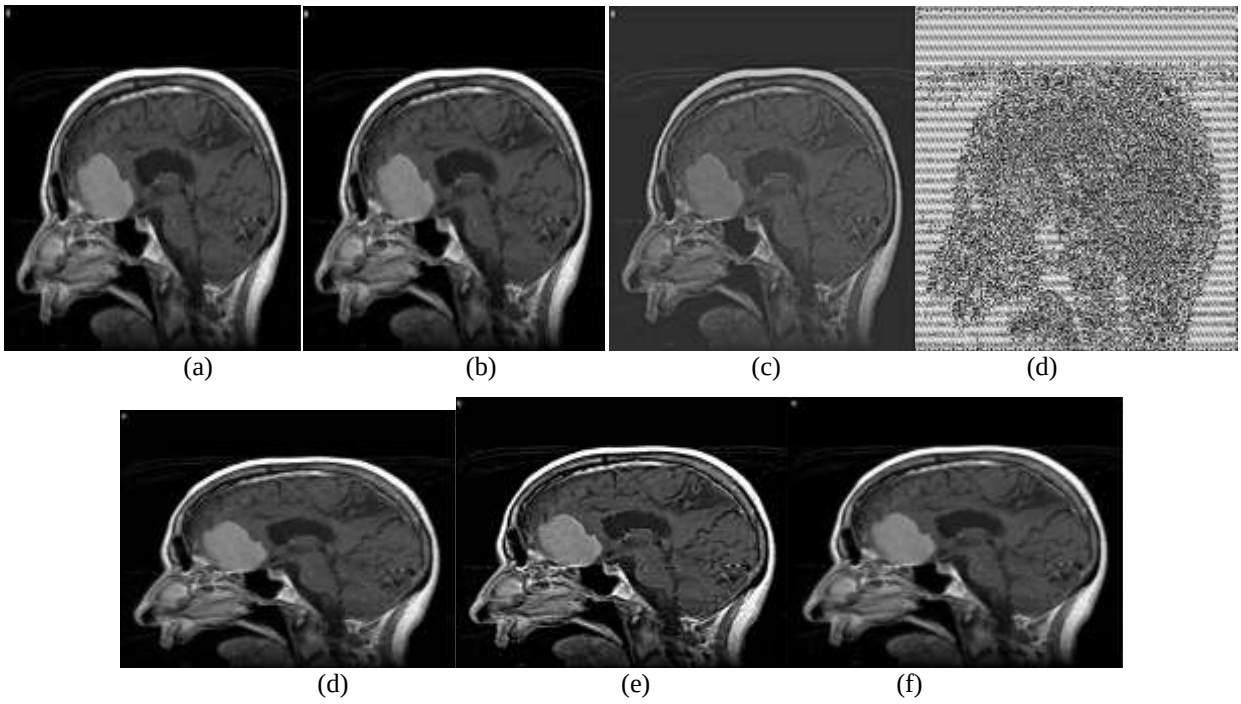

Figure 7: MBKGD-LBG Algorithm based Medical Brain Image Sample 4 (a) Input Image (b) Wavelet Decomposed Image (c) Compressed Image (d) Encrypted Image (e) Decrypted Image (f) Decompressed Image (g) Wavelet Reconstructed Image

DOI: 10.37200/IJPR/V24I5/PR201800
Received: 13 Feb 2020 | Revised: 07 Mar 2020 | Accepted: 23 Mar 2020

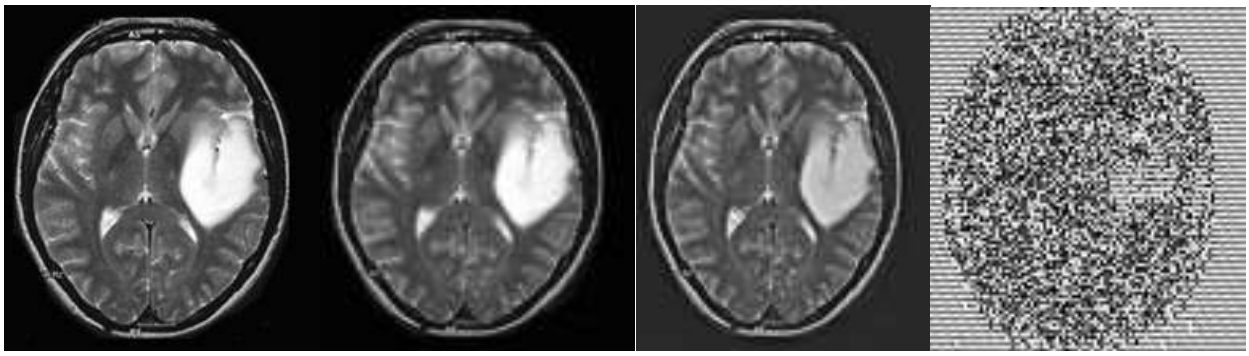

(a) (b) (c) (d)

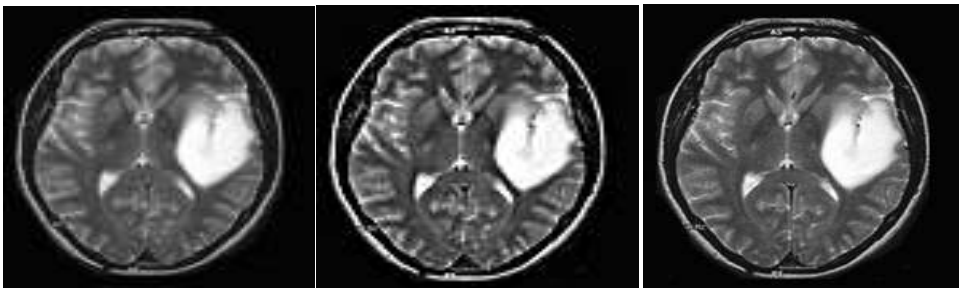

(d) (e) (f)

Figure 8: MBKGD-LBG Algorithm based Medical Brain Image Sample 5 (a) Input Image (b) Wavelet Decomposed Image (c) Compressed Image (d) Encrypted Image (e) Decrypted Image (f) Decompressed Image (g) Wavelet Reconstructed Image

The input image is decomposed using Discrete Wavelet Transform. Here, 'haar' wavelet is used to perform the decomposition process. The medical images are compressed using LBG (Linde, Buzo, and Gray) method. Then, the image encryption is done by using Multi-round Binary key generation with Diffusion method (MBKGD).

Five MRI grey scale standard test medical images are shown in Figure 4 to 8 for experiments and comparisons. The original input medical MRI image is shown in (a) section. The input image is decomposed using wavelet (Haar) shown in Figure (b). The LBG compressed image is shown in figure (c). The MBKGD encryption medical image is shown in Figure (d). MBKGD decrypted image is shown in figure (e) and LBG decompressed image is shown in figure (f). The reconstructed image is shown in Figure (g).

Performance Evaluation and Comparison of the Proposed MBKGD -LBG Method

For the purpose of performance analysis and comparison of the MBKGD-LBG method, five parameters are used. Finally, the compressed image size, encryption and decryption times are analyzed.

Table 1: Performance Evaluation of Proposed Method for CT Images

Sample	**PSNR (db)**	**MSE**	**SSIM**	**CR**	**BPP**
Brain CT1	52.2065	0.3596	0.9894	6.7997	0.425
Thorax CT2	55.2197	0.0969	0.9807	6.0097	0.3756
Liver CT3	59.0926	0.065	0.9794	7.212	0.4508

DOI: 10.37200/IJPR/V24I5/PR201800
Received: 13 Feb 2020 | Revised: 07 Mar 2020 | Accepted: 23 Mar 2020

Tables 1 and 2 give the performance evaluation of proposed method in CT and MRI images. Here, 5 CT and MRI images are taken and calculated the compression ratio, bpp, SSIM, MSE as well as PSNR values. The compression ratio is high shows that the compression performance is high because the prediction efficiency is better on edges. The average value of sample image of CT and MRI image parameters are calculated. The PSNR values and the bpp values are good since the CT and MRI medical images have homogeneous structure, the proposed method provides better compression quality and better bit rate reduction.

Table 2 Performance Evaluation of Proposed Method for MRI Images

Sample	PSNR (db)	MSE	SSIM	CR	BPP
Abdominal CT4	53.4331	0.1344	0.9831	6.3297	0.3956
Heart CT5	57.72	0.0672	0.977	7.1259	0.4454
Avg	**55.5344**	**0.1446**	**0.9819**	**6.6954**	**0.4185**
Abdominal MRI1	57.0103	0.0604	0.9861	6.5025	0.4064
Brain MRI2	56.527	0.1047	0.9936	5.6664	0.3541
Knee MRI3	62.7646	0.0168	0.9995	4.8571	0.3036
Spinal cord MRI4	59.0217	0.0645	0.9714	10.1692	0.6356
Thorax MRI5	53.009	0.117	0.9641	6.7227	0.4202
Avg	**56.4754**	**0.0872**	**0.9826**	**6.7835**	**0.4239**

Table 3: Response Time of Proposed Method for CT Images

Sample	PSNR (db)	MSE	SSIM	CR	BPP
Brain CT1	52.2065	0.3596	0.9894	6.7997	0.4250
Thorax CT2	55.2197	0.0969	0.9807	6.0097	0.3756
Liver CT3	59.0926	0.0650	0.9794	7.2120	0.4508
Abdominal CT4	53.4331	0.1344	0.9831	6.3297	0.3956
Heart CT5	57.7200	0.0672	0.9770	7.1259	0.4454
Avg	**55.5344**	**0.1446**	**0.9819**	**6.6954**	**0.4185**

Tables 3 and 4 give the performance evaluation of proposed method in CT and MRI images. Here, 5 CT and MRI images are taken and calculated the encryption and decryption time of the medical CT and MRI images. The response times are expressed in unit of seconds. The average value of sample image of CT and MRI image parameters are calculated.

Table 4: Response Time of Proposed Method for MRI Images

Sample	Encryption Time (sec)	Decryption Time (sec)	Total time (sec)
Abdominal MRI1	77.7554	76.8541	165.036798
Brain MRI2	56.6647	99.3544	156.0191
Knee MRI3	62.5589	123.4437	186.0026
Spinal cord MRI4	28.2704	31.6938	56.9642
Thorax MRI5	28.1865	58.2741	86.4606
Avg	**50.6871**	**77.9240**	**128.6111**

Table 5: Original and Compressed Image Size of Proposed Method for CT Images

Sample	Image Size (row x column)	Original image size (bits)	Compressed image Size (bits)
Brain CT1	350 x 437	38325	5636.25
Thorax CT2	395 x 493	48906	8137.8
Liver CT3	431 x 329	35640	4941.75
Abdominal CT4	457 x 375	43052	6801.5714
Heart CT5	367 x 333	30728	4312.1786
Avg	**400 x 394**	**39331**	**5965.91**

DOI: 10.37200/IJPR/V24I5/PR201800
Received: 13 Feb 2020 | Revised: 07 Mar 2020 | Accepted: 23 Mar 2020

Tables 5 and 6 give the performance evaluation of proposed method in CT and MRI images. Here, 5 CT and MRI images are taken and calculated the size of the original and compressed image. The compressed image is very helpful for security and also save the bandwidth needed to transfer the images. Here, the input image having different size, so the compression amount also different for each and every images.

Table 6: Original and Compressed Image Size of Proposed Method for MRI Images

Sample	Image Size (row x column)	Original image size (bits)	Compressed image Size (bits)
Abdominal MRI1	365 x 365	33489	5150.1429
Brain MRI2	420 x 525	55230	9747
Knee MRI3	490 x 612	74970	15435
Spinal cord MRI4	233 x 291	17082	1679.7857
Thorax MRI5	353 x 353	31329	4660.1571
Avg	**372 x 429**	**42420**	**7334.567**

Table 7 shows the comparison average values of structural similarity index and here 5 test images are compared with the proposed method. By comparing different methods such as CABAC, EZW, WDR and SPIHT with the proposed method the values are high in proposed method by comparing different existing methods in Ammah et al (2019). This shows that the perceived quality of the predicted image is better and the similarity between the original image and the reconstructed image are good for the proposed system. Then the average value of it is 0.9837.

Table 7: Comparison of Structural Similarity Index Method

TEST IMAGES	SSIM					
	CABAC	EZW	WDR	SPIHT	DWT-VQ	Proposed MBKGD -LBG Method
Brain CT1	0.6158	0.5366	0.62.2	0.5922	0.7632	0.9894
Thorax CT2	0.6874	0.6874	0.5832	0.6627	0.7689	0.9807
Liver CT3	0.5169	0.6169	0.5669	0.7146	0.7115	0.9794
Abdominal CT4	0.6867	0.7167	0.7260	0.7443	0.7932	0.9831
Heart CT5	0.7554	0.7554	0.6617	0.6508	0.7748	0.9861
Average	**0.6643**	**0.6719**	**0.6596**	**0.6801**	**0.7724**	**0.9837**

The PSNR values for the sample CT images are compared with SPIHT, EZW, SQP and WQT methods which are shown in Table 8. The average value of proposed method is 55.3924.The table reports that the proposed method provides better PSNR values when compared with SPIHT, EZW, SQP and WQT methods. Since the PSNR value of the proposed method is good, the perceptual image quality is high.

Table 8: Comparison of PSNR Values for CT Images with Existing Methods

Images	SPIHT	EZW	SQP	WQT	DWT-VQ	Proposed MBKGD -LBG Method
Brain CT1	45.82	45.60	45.43	45.90	30.9619	52.2065
Thorax CT2	33.62	33.17	33.35	33.57	24.1286	55.2197
Liver CT3	32.04	32.53	32.65	32.81	27.7495	59.0926
Abdominal CT4	30.80	30.23	30.55	30.70	26.3682	53.4331
Heart CT5	28.61	28.37	28.46	28.05	28.0147	57.0103
Average	**31.03**	**30.906**	**31.099**	**31.158**	**28.1181**	**55.3924**

The PSNR values for the sample MRI images are compared with SPIHT, EZW, SQP and WQT methods which are shown in Table 9. The table reports that the proposed method provides better PSNR values when compared with SPIHT, EZW, SQP and WQT methods. Since the average PSNR value for MRI of the proposed method is 56.4754, the perceptual image quality is high when compared to these methods.

DOI: 10.37200/IJPR/V24I5/PR201800
Received: 13 Feb 2020 | Revised: 07 Mar 2020 | Accepted: 23 Mar 2020

Table 9: Comparison of PSNR Values for MRI Images with Existing Methods

Images	SPIHT	EZW	SQP	WQT	DWT-VQ	Proposed MBKGD -LBG Method
Abdominal MRI1	51.21	51.52	52.03	52.43	53.01	51.0547
Brain MRI2	50.62	51.43	51.60	50.84	50.52	56.5270
Knee MRI3	45.72	45.07	46.21	46.09	47.16	62.7646
Spinal cord MRI4	42.45	43.36	42.63	43.51	40.25	59.0217
Thorax MRI5	37.53	36.38	37.06	36.64	44.12	53.0090
Average	**41.113**	**41.178**	**41.506**	**41.67**	**41.92**	**56.4754**

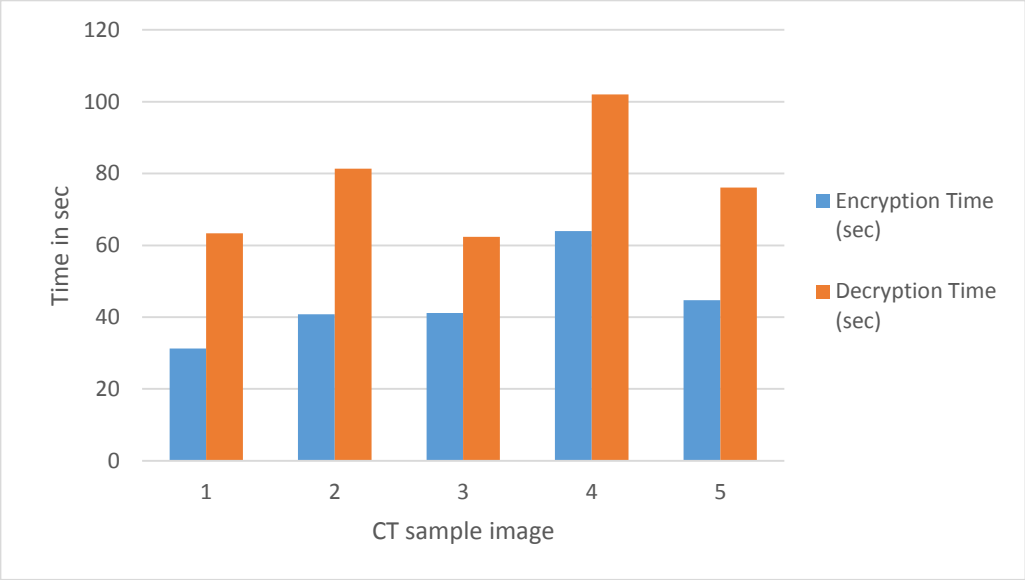

Figure 9: Response Time of MBKGD-LBG CT Medical Image

Figure 9 and 10 shows the graphical representation of encryption and decryption time of the MBKGD-LBG algorithms CT and MRI medical sample images. The response time is expressed in seconds.

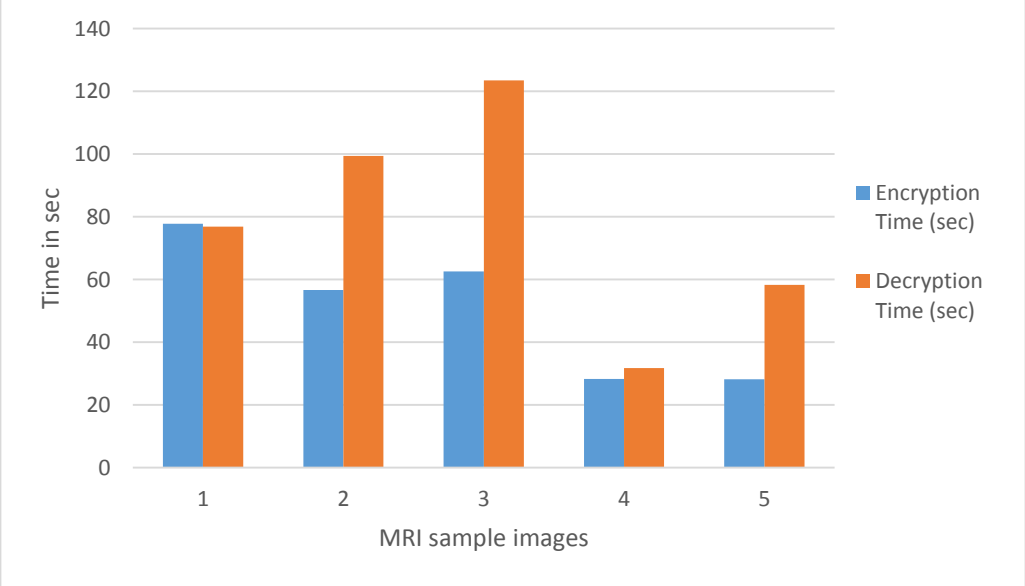

Figure 10: Response Time of MBKGD-LBG MRI Medical Image

DOI: 10.37200/IJPR/V24I5/PR201800
Received: 13 Feb 2020 | Revised: 07 Mar 2020 | Accepted: 23 Mar 2020

IV. CONCLUSION

In this thesis Multidirectional Oriented Prediction (MOP) scheme based on least square estimation is used to provide better near-lossless compression improvements and to overcome smaller bit rate reduction, to improve the perceptual fidelity in edges and to reduce the decoding time. MOP predictors are used to improve the prediction efficiency. The improvements achieved by the use of MOP results not only in a higher prediction gain but also improve high perceptual fidelity in edges in the predicted blocks by applying predictions in different orientations. In near lossless compression some distortion is allowed without affecting any data. Efficient compression is obtained using Huffman coding to increase the bit rate reduction. In order to predict the weak edges, sharp horizontal edges, sharp vertical edges as well as smooth areas in the medical images MOP is used along with Gradient Adjusted Prediction named MGOP. MGOP is used along with Hadamard transform to remove the blocking artifacts. Better performance in terms of compression ratio, PSNR values and bit rate reduction can be achieved by using vector based recursive crack coding image compression. Security is also a matter of concern in case of medical images where the privacy of patient records has to be maintained. In order to achieve security over hacking and to provide authentication, Compression-Then-Encryption based method is applied which uses vector based recursive crack coding image compression and honey encryption. The perceptual qualities of the output images are high since the PSNR values are high. The encryption and decryption time are less when compared to the existing algorithm which indicates that the execution time is less for secured transmission. Furthermore, the qualities of the encrypted images are high for the medical images. The result shows that high level of security has been retained for the secured transmission of compressed medical images. The proposed method also provides security beyond the brute-force attack.

REFERENCES

[1] Li Hui Fang, Miao, "Images Compression Using Dual Tree Complex Wavelet Transform", *International Conference of Information Science and Management Engineering,* 2010.

[2] Meng Meng; Meijuan Zong, "A new zero tree structure for color image compression based on DWT and VQ", *Information Management and Engineering (ICIME), 2010 The 2nd IEEE International Conference on*, vol., no., pp.339, 342, 16-18 April 2010.

[3] Nikkoo Khalsa, Dr. G. G. Sarate, Prof. D. T. Ingole, "Evaluation of factors affecting the selection of mother wavelet to improve image compression of Artificial & Natural Images", *IJC St Volume.*1, Issue 2, December 2010.

[4] Samir, K.B., Tuhin, U.P. and Avishek, R. "Image Compression using Approximate Matching and Run Length", *International Journal of Advanced Computer Science and Applications,* Vol. 2, No. 6, pp. 117-121,2011.

[5] Kalaivani K., Thirumaraiselvi, C., Sudhakar, R., "An effective way of image compression using DWT and SOM based vector quantization," *Computational Intelligence and Computing Research (ICCIC),* 2013 *IEEE International Conference* on, vol., no., pp.1,5, 26-28 December. 2013.

[6] Raid, W.M.Khedr, M. A. El-dosuky and Wesam Ahmed, "Jpeg Image Compression Using Discrete Cosine Transform - A Survey", *International Journal of Computer Science & Engineering Survey* Vol.5, No.2, April 2014.

[7] Han Seung Jang, Kuk Yeol Bae, Hong-Shik Park, and Dan Keun Sung. "Solar power prediction based on satellite images and support vector machine." *IEEE Trans. Sustain.* Energy 7, no. 3 (2016): 1255-1263.

[8] Hyeonwoo Cho, Juhyun Pyo, and Son-Cheol Yu. "Drift error reduction based on the sonar image prediction and matching for underwater hovering." *IEEE Sensors Journal 16*, no. 23 (2016): 8566-8577.

[9] Begaint Jean, Dominique Thoreau, Philippe Guillotel, and Christine Guillemot. "Region-Based Prediction for Image Compression in the Cloud." *IEEE Trans. Image Processing 27,* no. 4 (2018): 1835-1846.

DOI: 10.37200/IJPR/V24I5/PR201800
Received: 13 Feb 2020 | Revised: 07 Mar 2020 | Accepted: 23 Mar 2020

[10] Jiao Licheng, Miaomiao Liang, Huan Chen, Shuyuan Yang, Hongying Liu, and Xianghai Cao. "Deep fully convolutional network-based spatial distribution prediction for hyperspectral image classification." *IEEE Transactions on Geoscience and Remote Sensing 55*, no. 10 (2017): 5585-5599.

[11] Xing Quan Fu, Bo-Cheng Liu, Yi-Yuan Xie, Wei Li, and Yong Liu. "Image Encryption-Then-Transmission Using DNA Encryption Algorithm and the Double Chaos." *IEEE Photonics Journal* 10, no. 3, pp 1-15, 2018.

[12] Anandakumar, H., & Umamaheswari, K. (2017). An Efficient Optimized Handover in Cognitive Radio Networks using Cooperative Spectrum Sensing. *Intelligent Automation & Soft Computing*, 1–8.

[13] Arafeen, D., Arifeen, N., Khaliq Bari, S., & Ahmed, M. (2016). Digital Forensic Examination of Mobile phone Data. *International Journal Of Advanced Engineering, Management And Science,* 2(7), 0926-0928.

[14] Arulmurugan, R., & Anandakumar, H. (2018). Early Detection of Lung Cancer Using Wavelet Feature Descriptor and Feed Forward Back Propagation Neural Networks Classifier. *Lecture Notes in Computational Vision and Biomechanics*, 103–110.

[15] Chitra, S., & Maheswari, J. (2018). Customer Satisfaction towards TVS Bharath Motors in Aundipatti. *International Research Journal of Management, IT and Social Sciences,* 5(2), 91-95.

[16] Desfiandi, A., Suman Rajest, S., S. Venkateswaran, P., Palani Kumar, M., & Singh, S. (2019). Company Credibility: A Tool To Trigger Positive Csr Image In The Cause-Brand Alliance Context In Indonesia. *Humanities & Social Sciences Reviews,* 7(6), 320-331.

[17] Diwakar1, K., & Kumar, D. (2015). Design and Weight Optimization of Engine Mounting Bracket. *International Journal Of Advanced Engineering Research And Science,* 2(8), 38-41.

[18] Dr. P. Suresh and Suman Rajest S (2019), "An Analysis of Psychological Aspects in Student-Centered Learning Activities and Different Methods" in *Journal of International Pharmaceutical Research* , Volume: 46, Issue 01, Page No.: 165-172.

[19] Dr. P.S. Venkateswaran, Dr. A. Sabarirajan, S. Suman Rajest And R. Regin (2019) "The Theory of the Postmodernism in Consumerism, Mass Culture and Globalization" in *The Journal of Research on the Lepidoptera* Volume 50 (4): 97-113

[20] Farhood, K., Vajeeha, S., Vardhan, D., & Gowd, D. (2015). Taguchi Design Optimization of Machining Parameters in CNC End Milling of NIMONIC 75. *International Journal Of Advanced Engineering Research And Science,* 2(8), 1-5.

[21] Haldorai, A., & Kandaswamy, U. (2019). Supervised Machine Learning Techniques in Intelligent Network Handovers. *EAI/Springer Innovations in Communication and Computing*, 135–154.

[22] Haldorai, A., & Ramu, A. (2018). An Intelligent-Based Wavelet Classifier for Accurate Prediction of Breast Cancer. *Intelligent Multidimensional Data and Image Processing*, 306–319.

[23] Haldorai, A., Ramu, A., & Murugan, S. (2018). Social Aware Cognitive Radio Networks. *Social Network Analytics for Contemporary Business Organizations*, 188–202.

[24] Haldorai, A., Ramu, A., & Murugan, S. (2018). Social Aware Cognitive Radio Networks. *Social Network Analytics for Contemporary Business Organizations*, 188–202.

[25] K.B. Adanov, S. Suman Rajest, Mustagaliyeva Gulnara, Khairzhanova Akhmaral (2019), "A Short View on the Backdrop of American's Literature". *Journal of Advanced Research in Dynamical and Control Systems,* Vol. 11, No. 12, pp. 182-192.

[26] Krishnaiah, T., & Gowd, P. (2015). Experimental Investigation on Four Stroke CI Engine Using Corn Oil As Fuel. *International Journal Of Advanced Engineering Research And Science,* 2(8), 31-37.

[27] Kumari, P., & Gujjar, R. (2015). Android App For Automatic Malware Detection via Reviews and Permissions. *International Journal Of Advanced Engineering Research And Science,* 2(8), 17-21.

[28] Macías, EIP, Cedeño, HAC, & Chávez, GMR (2018). Importance of Improving Resilience in Teaching-Learning Process of Students with Disabilities. *International Research Journal of Management, IT and Social Sciences,* 5 (2), 120-128.

[29] Macías, T. M. D., Barreiro, L. M. Álava, & García, D. S. V. (2018). Challenges to Foster Resilience. *International Research Journal of Management, IT and Social Sciences,* 5(2), 80-90.

[30] Malarvizhi, J., & Devi, T. C. (2018). A Study on Customer Satisfaction towards Patanjali Products in Theni District. *International Research Journal of Management, IT and Social Sciences,* 5(2), 75-79.

[31] Md. Salamun Rashidin, Sara Javed, Bin Liu, Wang Jian, Suman Rajest S (2019), "Insights: Rivals Collaboration on Belt and Road Initiatives and Indian Recourses" in *Journal of Advanced Research in Dynamical and Control Systems,* Vol. 11, SI. 04, Page No.: 1509-1522.

[32] Mora, M. L. C., & Triana, M. S. F. (2018). The Management of Process of the Budget Area. *International Research Journal of Management, IT and Social Sciences,* 5(2), 104-112.

DOI: 10.37200/IJPR/V24I5/PR201800
Received: 13 Feb 2020 | Revised: 07 Mar 2020 | Accepted: 23 Mar 2020

[33] Motiwala, B. (2016). Role of Emotional Branding and Doppelganger Brand Image in Indian Lower House Elections of 2014. *International Journal Of Advanced Engineering, Management And Science,* 2(7), 0944-0951.

[34] Nohria, R., & Singh Mann, P. (2015). Adaptive Neuro-fuzzy Inference System for Hypertension Analysis. *International Journal Of Advanced Engineering Research And Science,* 2(8), 22-15.

[35] Rajest, S. S., Suresh, D. (2018). The Deducible Teachings of Historiographic Metafiction of Modern Theories of Both Fiction and History. *Eurasian Journal of Analytical Chemistry*, 13(4), emEJAC191005.

[36] Raunaque, N., Imam, M., & Raja, M. (2016). E-Commerce - Customer Experience and Relationship. *International Journal Of Advanced Engineering, Management And Science,* 2(7), 913-917.

[37] Roshini, A., & Anandakumar, H. (2015). Hierarchical cost effective leach for heterogeneous wireless sensor networks. *2015 International Conference on Advanced Computing and Communication Systems.*

[38] Sharma, A. (2015). Goods and Service Tax – The Journey so far. *International Journal Of Advanced Engineering Research And Science,* 2(8), 14-16.

[39] Singh, S. (2015). Analysis of Brake-Pad Friction Material Formulation. *International Journal Of Advanced Engineering Research And Science*, 2(8), 6-13.

[40] Suganya, M., & Anandakumar, H. (2013). Handover based spectrum allocation in cognitive radio networks. *2013 International Conference on Green Computing, Communication and Conservation of Energy (ICGCE).* doi:10.1109/icgce.2013.6823431

[41] Suman Rajest S, Dr. P. Suresh (2018), "Absurd Realism And Structure In Thomas Pynchon's The Crying Of Lot 49" in *Journal of Advanced Research in Dynamical and Control Systems,* Vol.10, SI.11, Page No.: 571-580.

[42] Suman Rajest S, Dr. P. Suresh (2019), "The Dialog On Postmodernism Intertextuality, Parody, The Talk Of History And The Issue Of Reference" in *International Journal of Recent Technology and Engineering,* Vol.7, Issue-5C, Page No.: 244-251.

[43] Suman Rajest S, Dr. P. Suresh, "An Analysis of Chetan Bhagat's Revolution -2020: Love, Ambition, Corruption" in *International Journal of English Language, Literature in Humanities,* Volume: V, Issue IX, September 2017, Page No.: 52-62.

[44] Suman Rajest S, Dr. P. Suresh, "Galapagos: Is Human Accomplishment Worthwhile" in Online *International Interdisciplinary Research Journal,* Volume: VII, Special Issue II, September 2017, Page No.: 307-314.

[45] Suman Rajest S, Dr. P. Suresh, "The white Tiger by Aravind Adiga: Depiction of Fermentation in Society" in *International Journal of Information Movement,* Volume: II, Special Issue VI, October 2017, Page No.: 189-194.

[46] Taneja, A., Kumar, S., Chaudhary, R., & Taneja, J. (2015). Optimization of Surface Roughness for AISI A2 on WEDM Using Response Surface Methodology. *International Journal Of Advanced Engineering Research And Science,* 2(8), 42-47.

[47] Toradmalle, D., & Banerjee, N. (2016). Disruption of Black Hole attacks in MANET. *International Journal Of Advanced Engineering, Management And Science,* 2(7), 0940-0943.

[48] Ur Rahim, M., Akhtar, S., & Bharti, D. (2016). Finite Element Analysis for the Buckling Load of Corrugated Tubes. *International Journal Of Advanced Engineering, Management And Science,* 6(7), 0935-0939.

[49] V.N, D., U.O., D., & Mcbarango, D. (2016). Effects of Poor Plants Management and Operator's Behaviour on Construction Site Health and Safety Performance. *International Journal Of Advanced Engineering, Management And Science,* 2(7), 918-925.

[50] Y.Sekhara, Y., H.Nahla, H., S.Elhasnaoui, S., M.Chergui, M., A.Chakir, A., & H.Medromi, H. (2016). Empirical Study on the Status of Moroccan Information Systems and Proposition of Approach for Choice of Best Practices for Good IT Governance. *International Journal Of Advanced Engineering, Management And Science,* 2(7), 0929-0934.

[51] Zambrano, R. L. B., Villamil, K. V. S., & Cantos, K. L. G. (2018). Resilience and Personal Improvement of Students with Motor Disabilities. *International Research Journal of Management, IT and Social Sciences,* 5(2), 96-103.

DOI: 10.37200/IJPR/V24I5/PR201800
Received: 13 Feb 2020 | Revised: 07 Mar 2020 | Accepted: 23 Mar 2020